# Railway ballast anisotropy testing via true triaxial apparatus

Zelong Yu[1,2,*], D. P. Connolly[3], P. K. Woodward[3], O.Laghrouche[2], E. Tutumluer[4],
[1] *Newcastle University, School of Civil Engineering & Geosciences, Newcastle Upon Tyne, NE1 7RU, UK*
*E-mail: Zelong.Yu@newcastle.ac.uk*
[2] *Heriot-Watt University, Institute for Infrastructure and Environment, Edinburgh, EH14 4AS, UK*
*E-mail: O.Laghrouche@hw.ac.uk*
[3] *University of Leeds, Institute for High Speed Rail and Systems Integration. Leeds, LS2 9JT, UK*
*E-mail: d.connolly@leeds.ac.uk; P.K.Woodward@leeds.ac.uk*
[4] *University of Illinois at Urbana-Champaign, Department of Civil and Environmental Engineering, 205 N. Mathews, Urbana, IL 61801, United States*
*E-mail: tutumlue@illinois.edu*

** Corresponding author*

## Abstract

This paper aims to demonstrate the anisotropic behaviour of railway ballast via true-triaxial tests. To do so, a novel, large-scale, true-triaxial testing apparatus (GeoTT) is designed and constructed. It consists of six hydraulic actuators, designed to apply a distributed stress to large granular cubic test specimens with dimensions: 500mm × 500m × 500mm. To show the capability of the new facility, crushed granite railway ballast with $d_{50}$=43mm is tested. Three different confining stresses are applied to determine the Poisson's ratio and modulus in three dimensions. Anisotropic behaviour is clearly evident, with horizontal directions showing a lower modulus compared to the vertical direction. It is also found that confining stress has an important effect on both Poisson's ratio and modulus when the primary loading is applied in three orthogonal directions. These results are useful for understanding the behaviour of railway ballast and for the calibration of railroad numerical models.

**Key words**: Granular particle anisotropy; Railway ballast; true triaxial testing (GeoTT), Ballast modulus; Poisson's ratio; Railroad

## 1 Introduction

Granular soils are often referred to as aggregates and are a common construction material for pavements and railways. A large number of studies have been undertaken to quantify the isotropic behaviour of granular particles, including [1–8]. Testing of granular materials with large maximum particle size requires a larger-scale testing appcccaratus compared to the testing of smaller particles. This is because larger sample volumes are required to ensure the ratio between maximum particle size and sample dimension is low.

Although isotropic loading tests provide insights into material behaviour, many granular materials actually behave in an anisotropic manner [9–12]. Table 1 outlines a range of studies performed using traditional triaxial cells to explore the anisotropy of response. The anisotropic behaviour of ballast is of significance for railway tracks because it aids the understanding of ballast behaviour in the horizontal direction. This is particularly important for tracks in curves. Further, it is an important material input when numerically modelling ballast.

However, investigating anisotropy ideally requires the test sample to be subject to a range of stress paths that are difficult to achieve using standard triaxial testing. Therefore, the two most common approaches to achieve this are: Hollow Cylinder Apparatus (HCA) and true triaxial (TT) testing. HCA methods are useful for simulating the rotation of principal stresses that occur during wheel passage. Alternatively, TT methods account for the effect of intermediate principal stresses, which in reality, may be different from the minor principal stresses when considering full anisotropy.

HCA works by subjecting a hollow, cylindrical soil sample to an axial load and torque about the central vertical axis, while applying external and internal radial pressures. The torque results in shear stress while the axial load combined with the radial pressures results in vertical stress [13–16].

The majority of HCA research into granular particle anisotropy to-date has focused on materials with relatively small maximum particle size (see Table 2). For example, Tatsuoka et al. [17], Pradhan et al. [18] and Pradhan et al. [19] tested soil specimens with an inner diameter, outer diameter and height of 60mm, 100mm and 200mm, respectively. They investigated the strength and deformation properties of Toyoura sand. Alternatively, Yang et al. [20] used larger HCA apparatus to investigate the anisotropic behaviour of saturated sand. Alternatively, Lade et al. [21] and Lade [22] used HCA tests to study the cross-anisotropic behaviour of Santa Monica beach sand and found that cross-anisotropy correlated with increasing inclinations of the major principal stress direction. O'Kelly and Naughton [23], O'Kelly and Naughton [24], Yang [25], Yang et al. [26] and Rolo [27] also used HCA testing to investigate the anisotropic behaviour of sands.

As an alternative to HCA testing, TT testing works by subjecting a soil sample to stresses in the three orthogonal planes, often using two hydraulic actuators in each plane, either via rigid flat plates or flexible membranes or a mixture of both (see Table 3 for a summary of previous studies). Sture and Desai [28] and Desai et al. [29] developed true triaxial test setups to apply a three-dimensional, independently controlled, and compressive stress state, using fluid or pneumatically pressurized flexible cushions to transmit stresses in three orthogonal directions, to a cubic sand-ballast specimen with dimensions 101.6mm × 101.6mm × 101.6mm. Isotropic loading was applied to specimens to determine anisotropic response behaviour (i.e., directional dependencies of compacted specimen responses). Alternatively, Yamada and Ishihara [30] used true triaxial apparatus with a cubic sand specimen of dimensions 100mm × 100mm × 100mm. Results indicated that behaviour was highly anisotropic, inherently due to grain orientation, size and shape. However, as the applied shear stress increased, at failure, the inherent anisotropic effects disappeared.

Alternatively, Reis et al. [31] developed a cubic triaxial cell to test 60mm specimens of saturated and unsaturated soil. Further, Ochiai and Lade [32] used true triaxial apparatus to study the anisotropic behaviour of Cambria sand and found that the major principal strain was the lowest when the dilation rate was at a maximum. The same apparatus was then used to develop a failure criterion for cross-anisotropic soils [33,34].

Furthermore, Tutumluer and Seyhan [35] and Seyhan and Tutumluer [36] used a triaxial device to test aggregate samples with 150 mm diameter and 150 mm height. The vertical modulus was found to be larger than the horizontal modulus for all tested aggregates except one gravel specimen which contained 16% fines (defined as passing the No. 200 sieve or smaller than 0.075 mm) in a dense-graded base course aggregate with a maximum size of 25 mm.

When testing granular particles, it is important to maximise the sample size-to-particle ratio, defined as the minimum dimension of the test sample divided by maximum particle size. If too small, individual particles dominate test results thus causing testing errors. As a guide, Nitchiporovitch [37] and Fagnoul and Bonnechere [38] suggested a minimum sample size-to-particle ratio of 5, while Marachi et al. [39] proposed a ratio of 6. Therefore, because the width of the HCA wall is relatively thin, it is not well-suited for testing large diameter particles. True triaxial apparatus is arguably better suited because it can house a cuboidal volume of granular material, with potentially larger dimensions than the HCA. However, even then, it is challenging to construct a TT apparatus of sufficient scale to investigate the anisotropy of samples containing large granular particles.

This paper addresses these sample size challenges by developing a new TT facility capable of testing soil samples with dimensions: 500mm x 500mm x 500mm. The large potential test volume means it is well suited to testing large-particle granular soils, including railway ballast. The maximum particle size tested in this study was 63mm, giving a sample size-to-particle ratio of approximately 8. The facility was used to apply tri-directional stress patterns to railroad ballast and investigate its anisotropic behaviour. Considering that previous research has focused on the relationship between confining stress and Poisson's ratio in the vertical direction only, this paper extends this concept to the relationship in the horizontal direction.

Table 1. Anisotropic tests conducted using traditional triaxial cells

| Source | Soil type | Dimension (mm) | Aim |
|---|---|---|---|
| Miura et al. [9] | Sand | Diameter =70mm, Height = 170mm | Anisotropy, stress-strain curves, liquefaction |
| Tutumluer and Seyhan [35] and Seyhan and Tutumluer [36] | Aggregate | Diameter =150mm Height =150mm | Anisotropy, resilient behaviour |

| | | | |
|---|---|---|---|
| Rolo [27] | Sand/clay | Diameter =100mm Height =200mm | Anisotropy, shear strength |
| Aursudkij et al. [40] | Ballast | Diameter =150mm Height =450mm | Resilient modulus and Poisson's ratio |
| Ngo et al. [41] | Ballast | Diameter =300mm Height =600mm | Anisotropy behaviour, mobilized friction angle |

Table 2. Anisotropic tests conducted using hollow cylinder apparatus

| Source | Soil type | Inner diameter/ Outer diameter/ Height (mm) | Aim |
|---|---|---|---|
| Hight et al. [14] | Sand/clay | 203/254/254 | Principal stress rotation effects |
| Tatsuoka et al. [17] | Sand | 30/50/200 | Anisotropy, shear strength |
| Pradhan et al. [18] and Pradhan et al. [19] | Sand | 60/100/200 | Anisotropy, shear strength |
| Grabe [16] | Sand | 60/100/200 | Principal stress rotation effects, anisotropy |
| Rolo [27] | Sand/clay | 76/100/200 | Anisotropy shear strength |
| Yang et al. [20] | Sand | 150/314/200 | Anisotropy, intermediate principal stress |
| Lade et al. [21] and Lade [22] | Sand | 180/220/400 | Principal stress rotation effects, anisotropy, Shear strength |
| O'Kelly and Naughton [23] and O'Kelly and Naughton [24] | Sand | 71/100/200 | Anisotropy, small strain, yield criterion |
| Yang [25] and Yang et al. [26] | Sand | 60/100/200 | Anisotropy, plasticity, non-coaxiality |

Table 3. Anisotropic tests conducted using true triaxial test apparatus

| Source | Soil type | Dimension of cubic sample side length (mm) | Aim |
|---|---|---|---|

| | | | |
|---|---|---|---|
| Yamada and Ishihara [30] | Sand | 100mm | Anisotropy, shear strength |
| Sture and Desai [28] and Desai et al. [29] | Sand/ballast | 101.6mm | Anisotropy, stress-strain curves |
| Ochiai and Lade [32] | Sand | 76mm | Anisotropy, stress-strain behaviour |
| Reis et al. [31] | Sand | 60mm | Anisotropy, saturated and unsaturated |
| GeoTT (present project) | Railway ballast | 500mm | Anisotropy, Poisson's ratio, modulus |

# 2 Apparatus development

## 2.1 True triaxial test rig

A true triaxial testing facility (hereafter called 'GeoTT') was designed for large granular particle testing in collaboration between Heriot Watt University and The University of Glasgow. It is 3.5m high and 1.85m wide, with the ability to house test samples with maximum lateral dimensions of 580mm (Figure 1). It consists of 6 independent hydraulic actuators, with 2 aligned in each Cartesian plane, making it well-suited for the large-scale testing of anisotropic behaviour (Figure 2). Also, using 6 rams instead of 3 means that a more uniform stress distribution can be applied to test samples. Thus, the effect of varying confining stress can be investigated. Each ram is connected to a load cell and a linear variable displacement transducer (LVDT) for control purposes. The control setup allows for a wide range of independent signal types to be fed into each ram.

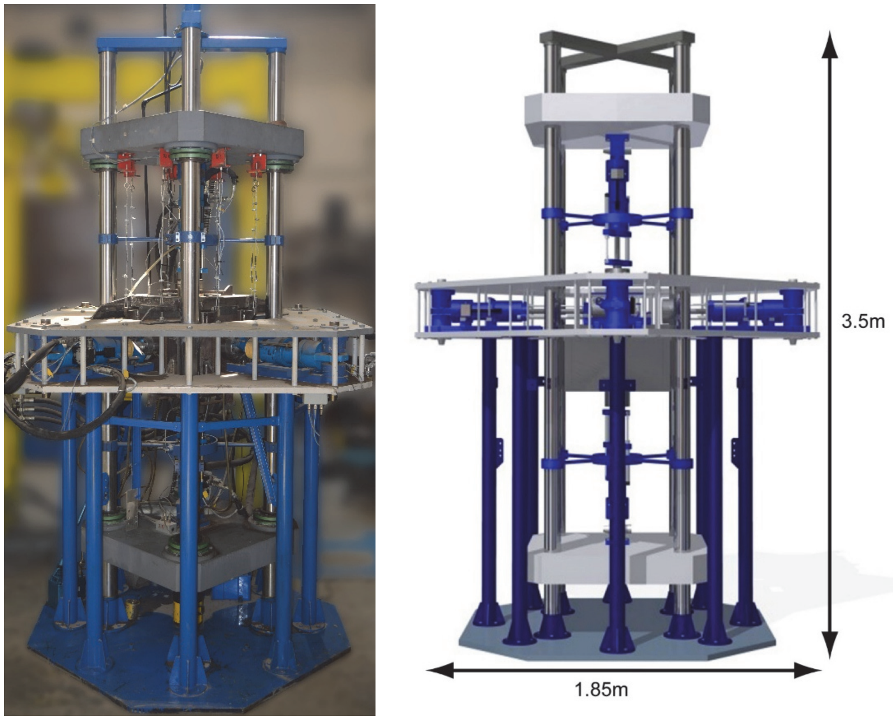


(a) (b)

*Figure 1. True triaxial testing apparatus: (a) Photograph, (b) Design drawing*

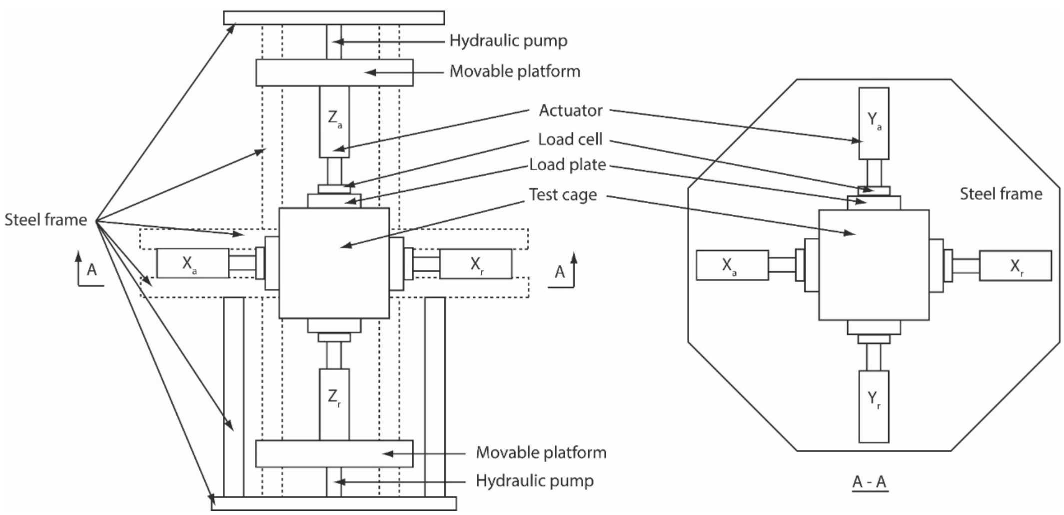


*Figure 2. Schematic of the GeoTT (Left: side view, Right Birdseye view – not to scale)*

## 2.2 Test cage

A bespoke steel test cage was developed to confine the large granular particles during testing. The outer skeleton had dimensions, 560mm x 560mm x 560mm, and 6 hollow sides. Each of these sides housed 6 separate and independently movable walls that allowed the sample to change volume during testing (Figure 3). Each wall had a maximum stroke of 60mm to prevent each wall colliding. The skeleton had protruding protective stops (not shown) to prevent sample egress in the event of excessive wall contraction (Figure 3a). These stops were linked to the control software and the test would automatically halt if this condition was reached. Further, to prevent small granular particles from exiting the sample via the skeleton-wall clearance, the inner test cage was encased using a thin plastic membrane (see Figure 4).

The true triaxial tests also depended upon the cage wall movement being independent from the cage skeleton. If friction was encountered at this location then the metal-on-metal contact could have introduced testing errors. During initial rig development, it was found that this friction risk was greatest in the vertical plane, due to potential sag of the horizontally orientated rams. Therefore a suspension system was developed to support the self-weight of the steel walls and load cells, thus counteracting the downward vertical force on the horizontal rams (Figure 5a). This was implemented by connecting the cage walls to the upper GeoTT frame via tuneable-length steel wires.

To illustrate the performance of the suspension system, Figure 5b shows a test performed during GeoTT commissioning, where the position of a lateral cage wall was cycled between the inside and outside of the cage skeleton. At the time prior to 800s (shown by the black line), the suspension system was not engaged, however, after 800s it was engaged. At all data points, the measured horizontal force was recorded to quantify the potential horizontal resistance due to friction. In absence of the suspension system, the force varied from -0.20kN to 0.12kN depending upon position, while when present the force varied from -0.09kN to 0.04kN. Therefore, when the suspension system was engaged, the friction between walls and cage skeleton was significantly reduced. Accordingly, the suspension system was used for all tests presented in this paper.

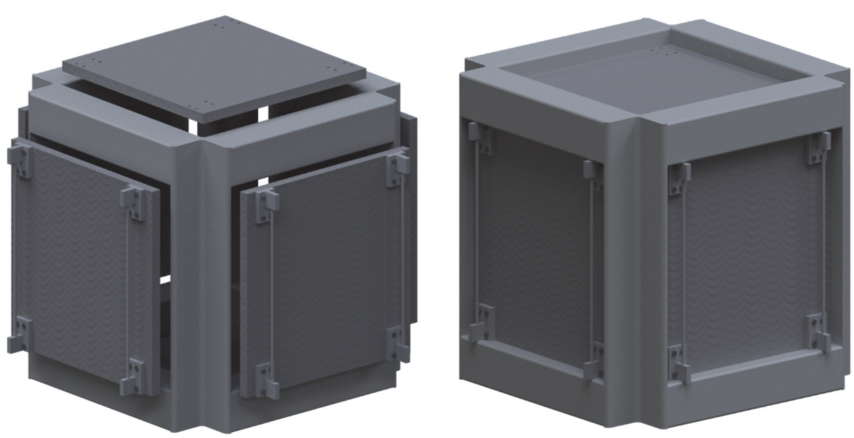

(a) (b)

Figure 3. GeoTT testing cage: (a) walls contracted, (b) walls compressed

*Figure 4. Inner cage with plastic sheet*

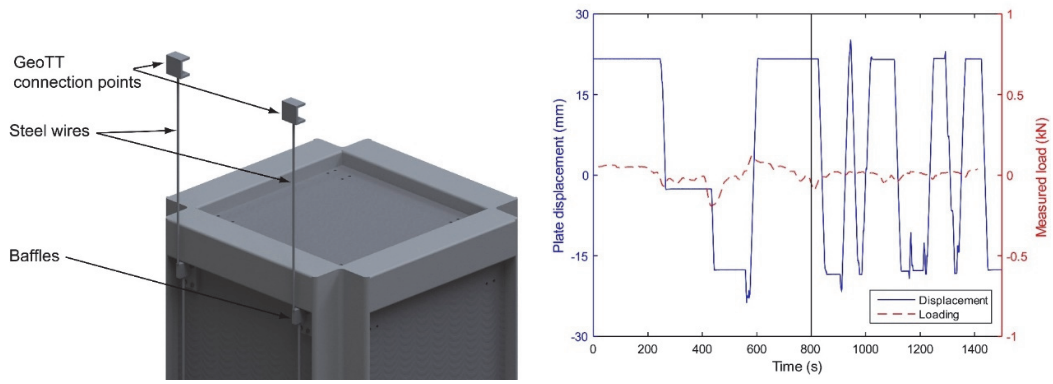


(a) (b)

*Figure 5. Suspension system details: (a) suspension design, (b) wall-skeleton friction*

# 3 Testing methodology

Two sets of tests were undertaken. First, monotonic axial loading tests were performed for the purpose of investigating the Poisson's ratio and modulus of ballast. Next, a combined hydrostatic loading and unloading test was performed to further investigate the cross-anisotropic behaviour of ballast. Both tests following independent loading plans.

## 3.1 Sample preparation

The particle size distribution (PSD) of the railway ballast material was characterised in accordance with BS EN 13450-2002 [42] / BS EN 13450-2013 [43], with all particles lying in the 20-63mm range and $d_{50}$ =43mm (see Figure 6). The coefficient of uniformity $C_u$ and coefficient of curvature $C_c$ were determined as 1.36 and 1.009 respectively, indicating the ballast was classified as uniformly graded. The ballast aggregate was also washed and dried in accordance with EN 13450-2002 [42] / BS EN 13450-2013 [43] and BS EN 933-1 [44]. After the ballast was prepared, it was poured into the test cage (500mm x 500mm x 500m) in 5 stages, and each layer was compacted for exactly 10 minutes using a vibrating Kango tool to achieve a specimen density of 1,300kg/m$^3$.

Although only particle size distribution tests were used to characterise the ballast, it was sourced from the same Network Rail approved quarry as the ballast used by Kwan [45]. Therefore the properties were likely to have been similar to those found in other UK ballast research works [e.g. LAA index $\leqslant$ 20 [46], MDE index $\leqslant$ 7 [47], ACV $\leqslant$ 22% [48], Flakiness index $\leqslant$ 35 [49], Particle length $\leqslant$ 4 [50]].

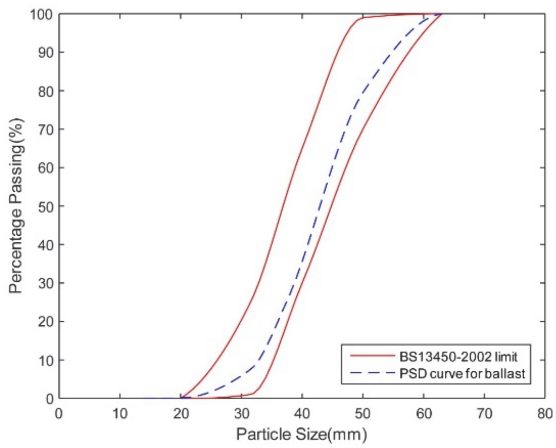


*Figure 6. Ballast particle size distribution curve*

## 3.2 Test 1: monotonic Axial Loading

The six rams ($X_a$, $X_r$, $Y_a$, $Y_r$, $Z_a$, $Z_r$) were used to apply static compressive stresses towards ballast samples as shown in Figure 7. Subscripts 'r' and 'a' are used to differentiate between the 2 different rams in each Cartesian plane. The axial load direction was varied between the X, Y and Z planes, and had a maximum value of 500kPa. Three different confining stresses (30, 60, 75kPa) were applied to the four specimen faces and each test (e.g. M1-9) was repeated three times, resulting in a total of 27 test results. The selection of these three confining stressed was based on the research from Indraratna et al. [51], where three degradation zones were identified with confining stress: less than 30kPa, 30-75kPa and larger than 75kPa. For each test, the following procedure, also summarized in Table 4, was used:

a) A constant confining stress (either 30kPa/60kPa/75kPa) was applied to the ballast sample in the 2 directions that were not the primary loading direction;
b) The position of the loading plate was recorded to determine the initial length of the sample (L);
c) An axial stress was applied in the primary loading direction and increased monotonically at a rate of 62.5kPa per minute, from an initial value of 6.25kPa. The opposite ram maintained a fixed position, thus creating a rigid

boundary;

d) When the axial stress reached 500kPa, it was held constant for 5 minutes;
e) The axial stress was decreased at a rate of 62.56kPa per 10 seconds until reaching a magnitude of 6.25kPa;
f) X, Y and Z displacements were recorded throughout steps a-e;
g) Steps a-f were repeated three times on the sample to ensure repeatability and consistency of results;
h) Steps a-g were repeated for the remaining axial loading directions; and finally,
i) The confining stress was increased (3 values tested: 30kPa/60kPa/75kPa) and steps a-h repeated.

*Table 4. Monotonic axial test procedure*

| Test stage | Confining stress (kPa) | Confining direction | Axial load direction | Rigid boundary |
|---|---|---|---|---|
| M1 | 30 | X and Y | Za | Zr |
| M2 | 30 | X and Z | Ya | Yr |
| M3 | 30 | Y and Z | Xa | Xr |
| M4 | 60 | X and Y | Za | Zr |
| M5 | 60 | X and Z | Ya | Yr |
| M6 | 60 | Y and Z | Xa | Xr |
| M7 | 75 | X and Y | $Z_a$ | $Z_r$ |
| M8 | 75 | X and Z | $Y_a$ | $Y_r$ |
| M9 | 75 | Y and Z | $X_a$ | $X_r$ |

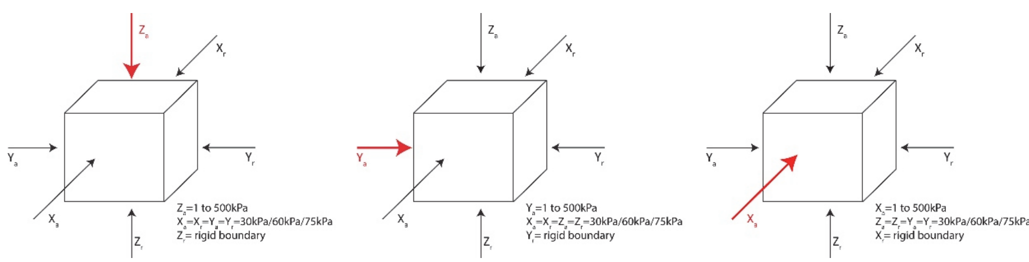


(a) (b) (c)

Figure 7. Axial load directions: (a) $Z_a$ loading, (b) $Y_a$ loading, (c) $X_a$ loading

## 3.3 Test 2: combined Hydrostatic Loading and Unloading

In addition to the monotonic axial loading tests, a combined hydrostatic loading and unloading test was also performed to investigate the unloading response of ballast. Rather than using the same procedure as for the previous monotonic tests (Table 4), the hydrostatic compression test procedure outlined by Desai et al. [29] was used and is summarized in Table 5:

a) A hydrostatic confining stress of 34.5kPa was applied in all 3 directions

b) The axial stress was increased in increments of 34.5kPa, from the confining stress (34.5kPa) to 172kPa. At each increment, the deformations were measured after they stabilized.
c) The axial stress was reduced from 172kPa to 34.5kPa in 34.5kPa increments
d) The axial stress was increased in increments of 34.5kPa, from the confining stress (34.5kPa) to 345kPa. At each increment, the deformations were measured after they stabilized.
e) The axial stress was reduced from 345kPa to 34.5kPa, in 34.5kPa increments
f) The axial stress was increased in increments of 34.5kPa, from the confining stress (34.5kPa) to 517kPa. At each increment, the deformations were measured after they stabilized.
g) The axial stress was reduced from 517kPa to 34.5kPa, in 34.5kPa increments;
h) The test was repeated for the remaining two Cartesian planes.

*Table 5.* Hydrostatic testing procedure

| Test stage | Confining stress (kPa) | Deviator stress (kPa) | Confining direction | Axial load direction | Rigid boundary |
|---|---|---|---|---|---|
| H1 | 34.5 | 137.5 | X and Y | $Z_a$ | $Z_r$ |
| H2 | 34.5 | 310.5 | X and Z | $Y_a$ | $Y_r$ |
| H3 | 34.5 | 482.5 | Y and Z | $X_a$ | $X_r$ |

## 3.4 Interpretation of test results

When a uniaxial compressive force is applied to a cubic or cuboidal test specimen, it contracts in the axial direction and expands in the remaining two perpendicular/transverse directions (Figure 8). Assuming the axial stress is in the Z direction, the resulting recoverable horizontal strains are in the X and Y directions (see Figure 9). For this case, Equations (1), (2) and (3) give the calculation for the axial recoverable strain in the Z direction and the horizontal (or transverse) recoverable strains in X and Y directions, respectively. Then, the magnitude of the average horizontal or transverse strain is calculated using Equations (4):

$$\varepsilon_{axial} = \frac{\delta_z}{L}, \text{ (positive for axial compression)} \qquad (1)$$

$$\varepsilon_{trans_x} = \frac{\delta_x}{L}, \text{ (negative for axial compression)} \qquad (2)$$

$$\varepsilon_{trans_y} = \frac{\delta_y}{L}, \text{ (negative for axial compression)} \qquad (3)$$

$$\varepsilon_{trans} = \frac{\varepsilon_{trans_x} + \varepsilon_{trans_y}}{2} \qquad (4)$$

Where,

L is the initial length of the ballast sample

$\delta_x$ is the recoverable displacement of ballast sample in X direction

$\delta_y$ is the recoverable displacement of ballast sample in Y direction

$\delta_z$ is the recoverable displacement of ballast sample in Z direction

Thus, Poisson's ratio is calculated as:

$$\nu = -\frac{\varepsilon_{trans}}{\varepsilon_{axial}} \qquad (5)$$

and the modulus is calculated as:

$$Modulus = \frac{\sigma_{axial\_time}}{\varepsilon_{axial\_time}} \qquad (6)$$

Where,

$\sigma_{axial\_time}$ is the axial stress time history

$\varepsilon_{axial\_time}$ is the axial strain time history

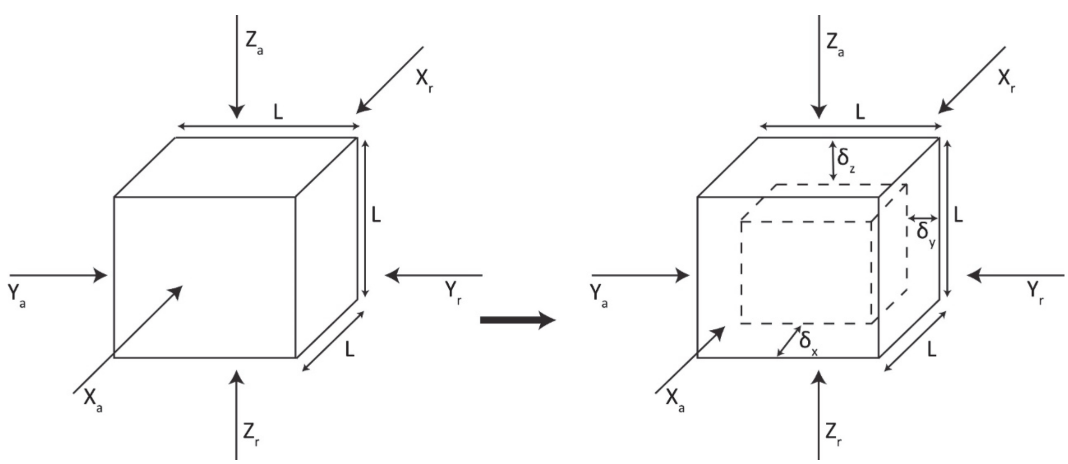


(a) (b)

Figure 8. Poisson's Ratio calculation: (a) un-deformed specimen, (b) deformed specimen in dashed line

# 4 Test results and discussion

## 4.1 Test 1 results

### 4.1.1 Poisson's ratio

For each confining stress and axial load pair, 3 tests were performed. As an example, Figure 9 shows the loading path and displacements in X, Y and Z directions for monotonic axial loading in the $Z_a$ direction under a confining stress of 75kPa. The displacements were used for the calculation of strains, while only recoverable strains were used for the calculation of Poisson's ratio. It is seen that deformation did not return to zero after unloading, thus indicating plastic deformation. This plastic deformation indicated that additional sample compaction occurred in the vertical direction and additional expansion in the horizontal direction, when the primary loading was applied in $Z_a$.

Since 3 repeated tests were performed under the same confining stress and axial load direction, the mean value of Poisson's ratio was calculated to minimize the test error (e.g. the 3 Poisson' ratios in the Za direction from stage M1 with 30kPa confining were averaged, giving a mean Poisson's ratio of 0.31).

Figure 10 shows the relationship between confining stress and Poisson's ratio.  It is seen that there was a distinct correlation, with Poisson's ratio decreasing with increased confining stress.  The mean values in X, Y and Z directions were 0.28, 0.32 and 0.31 at a confining stress of 30kPa. The Poisson's ratio values reduced to 0.22, 0.26 and 0.23 for a confining stress of 60kPa and further reduced to 0.15, 0.19 and 0.18 for a confining stress of 75kPa (Table *6*). This is primarily because the increased confining stress reduced the displacement in the confining direction, resulting in a lower Poisson's ratio. This was consistent with the ballast triaxial tests performed by Indraratna et al. [52], where the initial loading stage was used for the study between confining stress and Poisson's ratio in the vertical direction. It was found that Poisson's ratio decreased with increasing confining stress. Similarly, Aursudkij et al. [40] carried out cyclic triaxial tests and found that the vertical Poisson's ratio decreased as confining stress increased from 30kPa to 60kPa under axial loading. The small discrepancies between the X and Y directions were likely because the monotonic test in the X direction was performed after the Y direction, resulting in a lower Poisson' ratio in the X direction.

Table 6. Poisson's ratios for monotonic lading in X, Y and Z directions

| Confining stress (kPa) | 30 | | | 60 | | | 75 | | |
|---|---|---|---|---|---|---|---|---|---|
| Axial load direction | X | Y | Z | X | Y | Z | X | Y | Z |
| Mean value of Poisson's ratio | 0.28 | 0.32 | 0.31 | 0.22 | 0.26 | 0.23 | 0.15 | 0.19 | 0.18 |

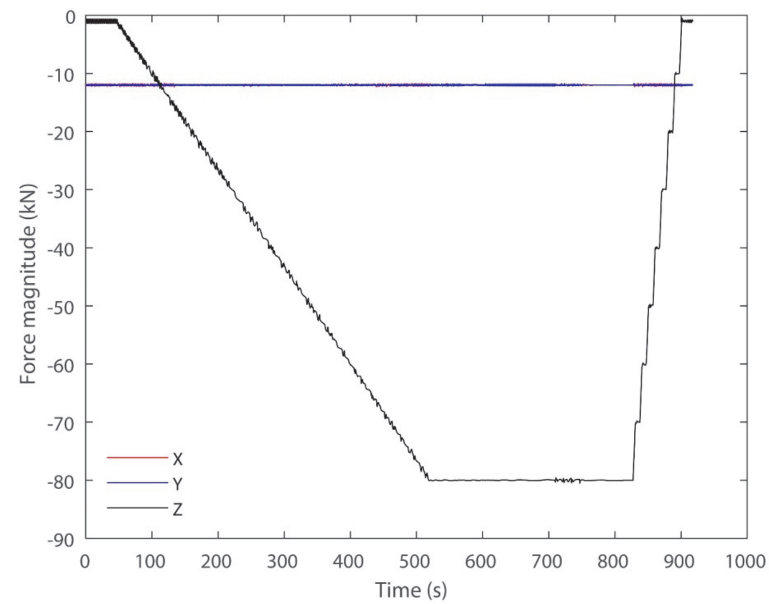


(a)

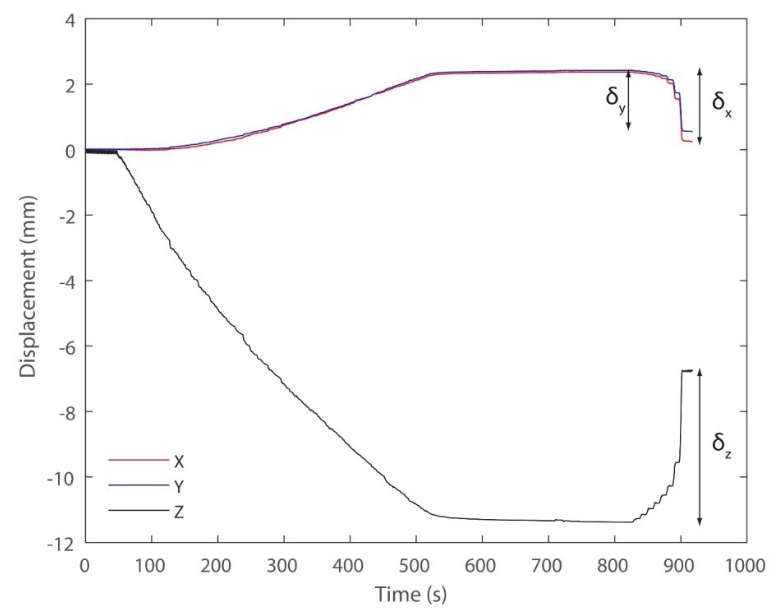


(b)

*Figure 9. Monotonic testing results when loading in $Z_a$ direction under a confining stress of 75kPa: (a) loading path, (b) displacements in X, Y and Z directions*

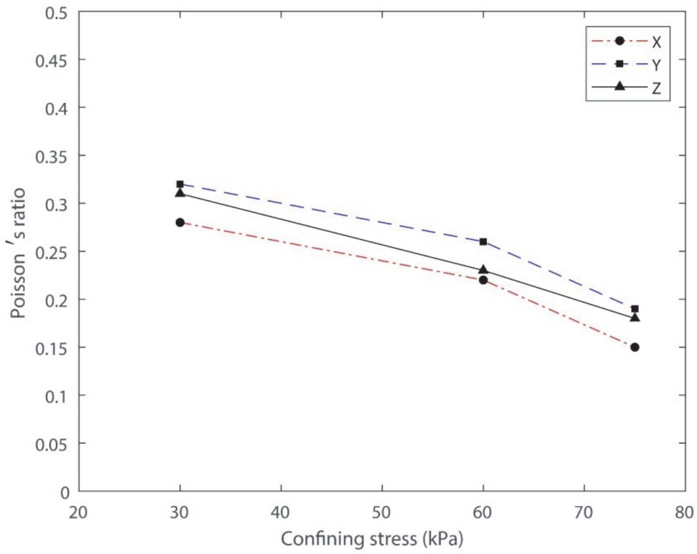


*Figure 10. Relationship between Poisson's ratio and axial loading direction*

### 4.1.2 Modulus

Figure 11 shows an example of the modulus from all repeated tests in X, Y and Z axial load directions under 75kPa confining stress. Correspondingly, Figure 12-Figure 14 show the mean modulus (average modulus across the 3 repeated tests) for confining stresses of 30, 60 and 75kPa respectively. Considering the Z direction at 30kPa, Figure 12 shows that the modulus decreased rapidly when the axial stress was low, reached a local minimum and then increased again steadily as axial stress was increased. This dilation resulted in the modulus at the end of the test (500kPa) being similar to the starting value. Regarding the X and Y directions, their responses were similar and had modulus significantly lower than the vertical direction (Z is on average 73% higher than X, and 66% higher than Y, when the axial stress is 500kPa). Horizontal modulus is particularly important on railway curves where lateral forces are higher compared to the straight track.

Similar findings were obtained for confining stresses of 60kPa and 75kPa. Figure 13 shows the 60kPa case where Z was on average 66% higher than X and 76% higher than Y when the axial stress was 500kPa. Alternatively, Figure 14 shows the 75kPa case where Z was on average 46% higher than X and 54% higher than Y when the axial stress was 500kPa. The overall combined results are shown in Figure 15 where it can be seen that for all directions, the lower confining stress resulted in lower modulus. This is important for railways because different locations within the ballast layer have different confining stress. Further, ballast layer dimensions vary across different lines, either due to design or historical maintenance procedures. Therefore different track sections also have different confining stresses.

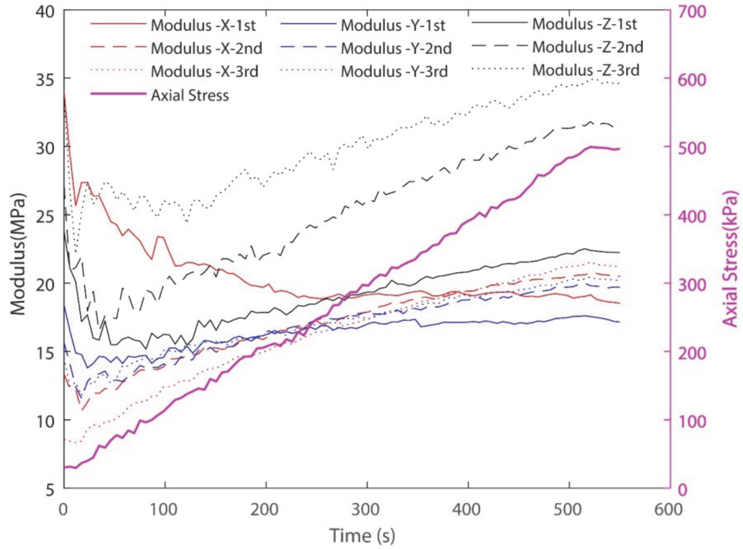


*Figure 11. Raw modulus in X, Y and Z axial load directions under 75kPa confining stress*

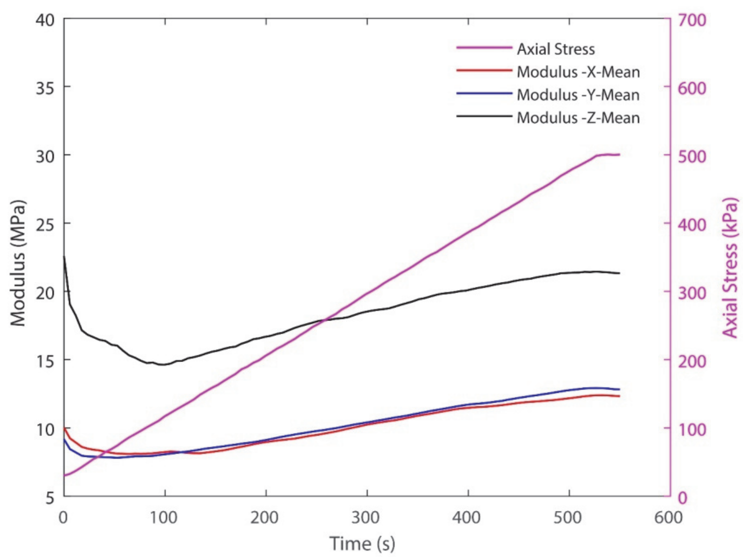


*Figure 12. Mean modulus in X, Y and Z axial load directions under 30kPa confining stress*

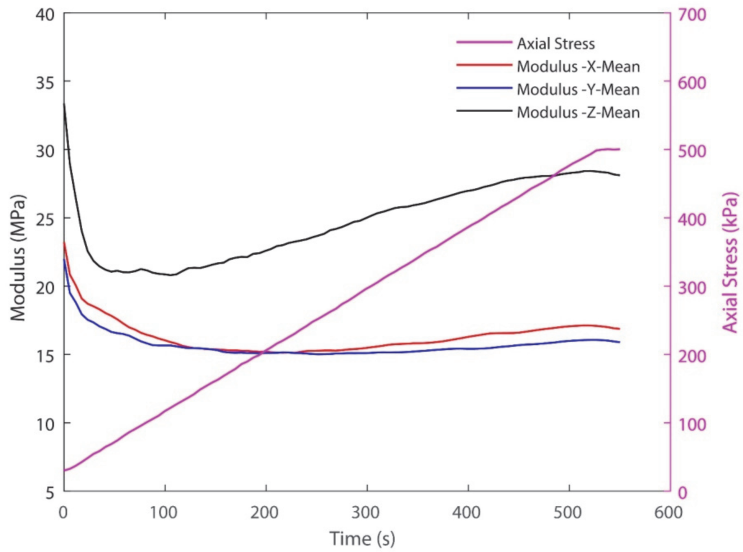


*Figure 13. Mean modulus in X, Y and Z axial load directions under 60kPa confining stress*

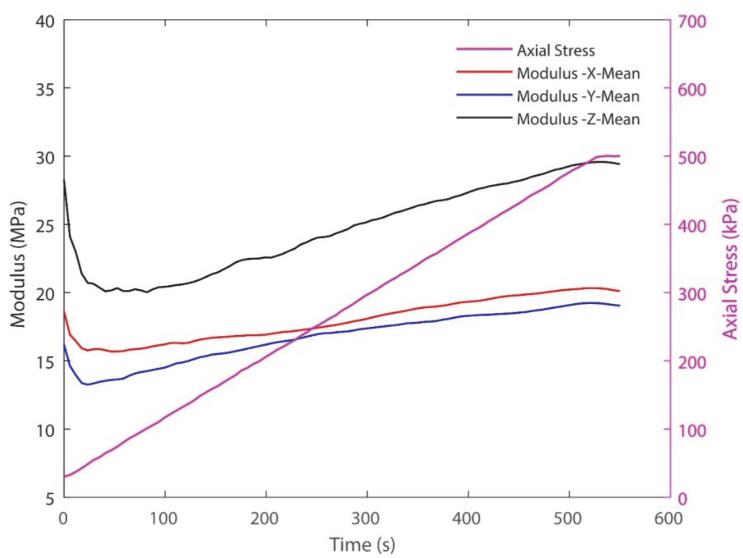


*Figure 14. Mean modulus in X, Y and Z axial load directions under 75kPa confining stress*

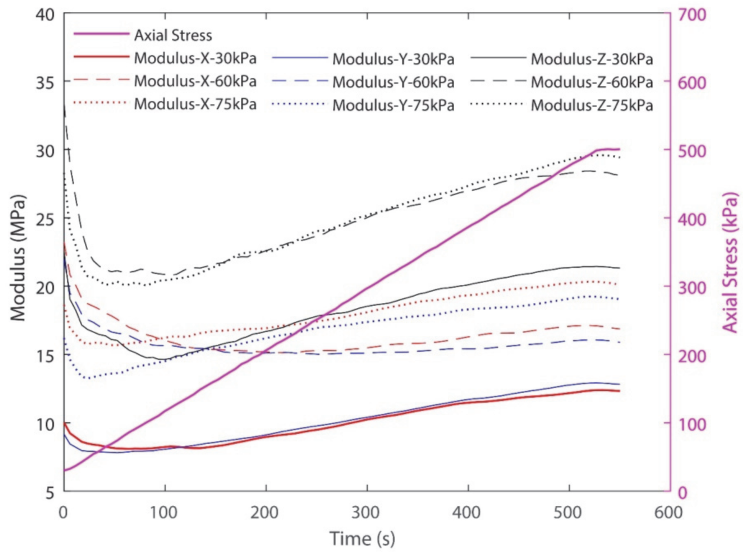


*Figure 15. Mean modulus in X, Y and Z axial load directions under varying confining stress*

## 4.2 Test 2 results

Figure 16 shows the three loading and unloading cycles of the test sample. Permanent deformation was clearly recorded after the 3 cycles in X, Y, and Z directions, and reached maximums of 172kPa, 345kPa and 517kPa, respectively. The horizontal directions (X and Y) exhibited approximately double the permanent deformation (3%) compared to the vertical direction (1.5%), thus demonstrating the typical cross-anisotropic behaviour of ballast. Based on recoverable strains after each unloading stage, the relationship between sample modulus and deviator stress is presented in Figure 17. It shows that sample modulus in the X and Y directions increased from 640 MPa and 600 MPa, to 800 MPa and 700MPa respectively, when the deviator stress was 310.5 kPa. However, the sample modulus in the Z direction increased from 900 MPa to 1000 MPa when deviator stress reached 310.5 kPa, and then remained constant. This change of modulus in each direction again indicated the cross-anisotropic behaviour of the ballast sample, while this cross-anisotropic behaviour was similar in X and Y direction in terms of unloading response and sample modulus. However, it should be noted that the responses show discrepancies with traditional nonlinear soil behaviour.

Upon inspection after testing, ballast breakage was noticed when removing the sample from the test cage. Also, ballast aggregate particle cracking was heard during testing.

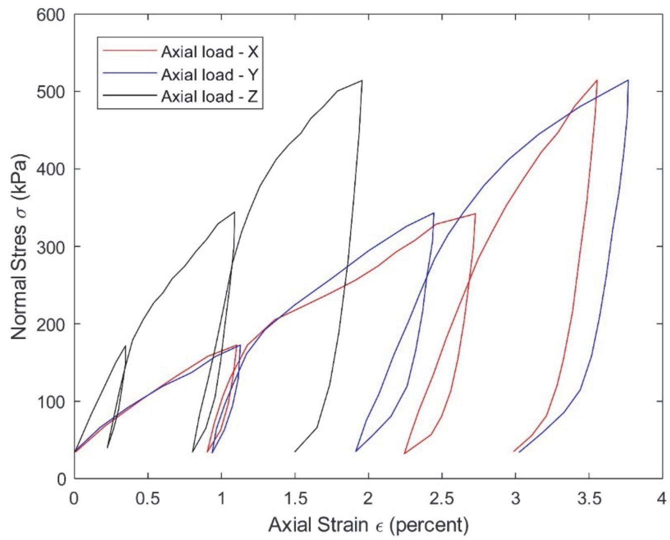


*Figure 16. Unloading response in all three axial load directions*

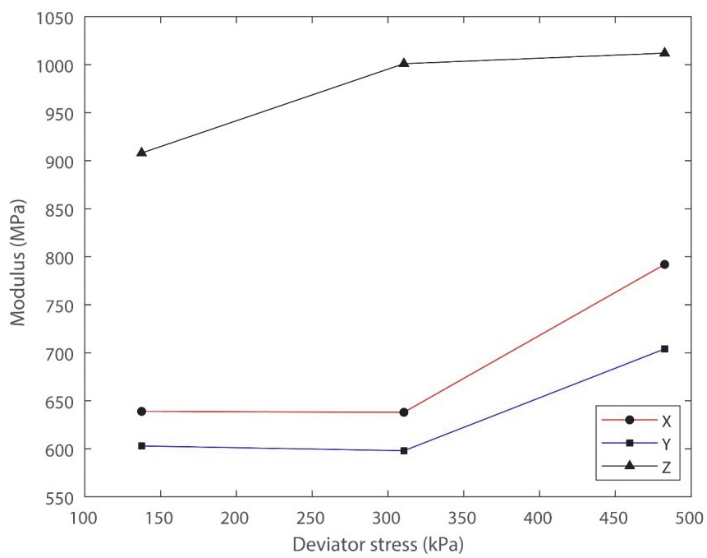


*Figure 17. Relationship between modulus and deviator stress*

# 5 Conclusions

Railway ballast typically behaves in an anisotropic manner, with greater stiffness in the vertical compaction direction. This is important to quantify for a better understanding of the field mechanical behaviour, and for the modelling of the dynamic response behaviour. Therefore, this paper presented results for a railway ballast aggregate material tested under true-triaxial conditions. A novel, large, true-triaxial apparatus and its accompanying testing cage were successfully developed in the laboratory. The true triaxial device utilised six hydraulic actuators to ensure a uniform stress distribution across the test sample. Three confining stresses (30kPa, 60kPa and 75kPa) were used to investigate Poisson's ratio, modulus and loading-unloading characteristics. Anisotropic behaviour was clearly observed for the ballast aggregate material; the horizontal response as obtained from horizontal and transverse strain measurements varied when compared to the strain values measured in the vertical direction. Both Poisson's ratio and modulus were sensitive to the applied confining stresses.

# 6 Acknowledgement

The authors express their gratitude to The University of Glasgow and Prof David Muir Wood for their significant efforts on the original development of the true triaxial rig. They also thank Heriot-Watt University for the support to modify the original design and adaption for ballast testing. Also, support from the University of Leeds is acknowledged along with the financial assistance from the Leverhulme Trust (PLP-2016-270).

# 7 References


[1] Roscoe KH, Schofield AN, Thurairajah A. Yielding of clays in states wetter than critical. Géotechnique 1963;13:211–40.

[2] Lade P V., Duncan JM. Elastoplastic stress-strain theory for cohesionless soil. ASCE J Geotech Eng Div 1975;101:1037–53.

[3] Van Eekelen HAM. Isotropic yield surfaces in three dimensions for use in soil mechanics. Int J Numer Anal Methods Geomech 1980;4:89–101.

[4] Sagaseta C. Analysis of undraind soil deformation due to ground loss. Géotechnique 1987;37:301–20.

[5] Alonso E., Gens A, Josa A. A constitutive model for partially saturated soils. Géotechnique 1990;40:405–30.

[6] Laloui L, Cekerevac C. Thermo-Plasticity of Clays: An Isotropic Yield Mechanism. Comput Geotech 2003;30:649–660.

[7] Rotta G V., Consoli NC, Prietto PDM, Coop MR, Graham J. Isotropic yielding in an artificially cemented soil cured under stress. Géotechnique 2003;53:493–501.

[8] Alonso EE, Pinyol NM, Gens A. Compacted soil behaviour: initial state, structure and constitutive modelling. Géotechnique, 2012;V1:134p.

[9] Miura, Seiichi and Toki S. Anisotropy in mechanical properties and its simulation of sands sampled from natural deposits. Soils Found 1984;24:69–84.

[10] Tutumluer E. Predicting behavior of flexible pavements with granular bases. PhD Thesis, Georgia Institute of Technology, 1995.

[11] Tutumluer E, Thompson MR. Anisotropic modeling of granular bases in flexible pavements. J Transp Res Board 1997;TRR 1577:18–26.

[12] Tutumluer E, Kwon J. Validations of Anisotropic Aggregate Base Behavior from Full-Scale Pavement Tests. Contemp Top Gr Modif Probl Soils, Geo-Support, Reston, VA: American Society of Civil Engineers; 2009, p. 441–8.

[13] Cooling LF, Smith DB. The Shearing Resistance of Soils. J Inst Civ Eng 1936;3:333–43.

[14] Hight DW, Gens A, Symes MJ. The development of a new hollow cylinder apparatus for investigating the effects of principal stress rotation in soils. Géotechnique 1983;33:355–83.

[15] Saada A. State-of-the-Art Paper: Hollow Cylinder Torsional Devices: Their Advantages and Limitations. Adv Triaxial Test Soil Rock, 100 Barr Harbor Drive, PO Box C700, West Conshohocken, PA 19428-2959: ASTM International; 1988, p. 766-766–24.

[16] Grabe PJ. Resilient and permanent deformation of railway foundations under principal stress rotation. PhD Thesis, University of Southampton, 2003.

[17] Tatsuoka F, Sonoda S, Hara K, Fukushima S, Pradhan TBS. Failure and deformation of sand in torsional shear. Soils Found 1986;26:79–97.

[18] Pradhan, T.B.S., Tatsuoka, F. and Horii N. Simple shear testing on sand in a torsional shear apparatus. Soils Found Japanese Soc Soil Mech Found Eng 1988;28:95–112.

[19] Pradhan, T.B.S., Tatsuoka, F. and Horii N. Strength and deformation characteristics of

sand in torsional simple shear. Soils Found 1988;28:131–48.

[20] Yang ZX, Li XS, Yang J. Undrained anisotropy and rotational shear in granular soil. Géotechnique 2007;57:371–84.

[21] Lade P V., Nam J, Hong WP. Shear banding and cross-anisotropic behavior observed in laboratory sand tests with stress rotation. Can Geotech J 2008;45:74–84.

[22] Lade P V. Failure Criterion for Cross-Anisotropic Soils. J Geotech Geoenvironmental Eng 2008;134:117–24.

[23] O'Kelly BC, Naughton PJ. Development of a new hollow cylinder apparatus for stress path measurements over a wide strain range. Geotech Test J 2005;28:345–54.

[24] O'Kelly BC, Naughton PJ. Study of the yielding of sand under generalized stress conditions using a versatile hollow cylinder torsional apparatus. Mech Mater 2009;41:187–98.

[25] Yang L. Experimental study of soil anisotropy using hollow cylinder testing. PhD Thesis, University of Nottingham, 2013.

[26] Yang LT, Li X, Yu HS, Wanatowski D. A laboratory study of anisotropic geomaterials incorporating recent micromechanical understanding. Acta Geotech 2016;11:1111–29.

[27] Rolo R. The anisotropic stress-strain-strength behaviour of brittle sediments. PhD Thesis, Imperial College London (University of London), 2004.

[28] Sture S, Desai CS. Fluid cushion truly triaxial or multiaxial testing device. Geotech Test J 1979;2:20–33.

[29] Desai CS, Siriwardane HJ, Janardhanam R. Interaction and load transfer through track support systems, Parts 2. Final Rep, DOT/RSPA/DMA-50/83/12, Off Univ Res Dept Transp Washington, DC 1983.

[30] Yamada Y, Ishihara K. Anisotropic deformation characteristics of sand under three dimensional stress conditions. Japanese Soc Soil Mech Found Eng 1979;19:79–94.

[31] Reis RM, de Azevedo RF, Botelho B, Severino N, Vilar OM. Performance of a cubical triaxial apparatus for testing saturated and unsaturated soils. Geotech Test J 2011;34:1.

[32] Ochiai H, Lade PV. Three-Dimensional Behavior of Sand with Anistropic Fabric. J Geotech Eng 1983;109:1313–28.

[33] Abelev A V, Lade P V. Effects of cross anisotropy on three-dimensional behavior of sand. I: Stress-strain behavior and shear banding. J Eng Mech 2003;29:160–6.

[34] Abelev A V., Lade P V. Characterization of Failure in Cross-Anisotropic Soils. J Eng Mech 2004;130:599–606.

[35] Tutumluer E, Seyhan U. Laboratory Determination of Anisotropic Aggregate Resilient Moduli Using an Innovative Test Device. Transp Res Rec J Transp Res Board 1999;1687:13–21.

[36] Seyhan U, Tutumluer E. Anisotropic Modular Ratios as Unbound Aggregate Performance Indicators. J Mater Civ Eng 2002;14:409–16.

[37] Nitchiporovitch AA. Shearing strength of coarse shell materials. Proc 7th Int Conf Soil Mech Found Eng Mex, 1969, p. 211–6.

[38] Fagnoul A, Bonnechere F. Shear strength of porphiry materials. Proc 7th Int Conf Soil Mech Found Eng Mex, 1969, p. 61–5.

[39] Marachi ND, Chan CK, Seed HB. Evaluation of properties of rockfill materials. J Soil Mech Found Div 1972;97.

[40] Aursudkij B, McDowell GR, Collop AC. Cyclic loading of railway ballast under triaxial conditions and in a railway test facility. Granul Matter 2009;11:391–401.

[41] Ngo NT, Indraratna B, Rujikiatkamjorn C. Micromechanics-Based Investigation of Fouled Ballast Using Large-Scale Triaxial Tests and Discrete Element Modeling. J Geotech Geoenvironmental Eng 2017;143:04016089.

[42] BSI. BS EN 13450 Aggregates for railway ballast. Br Stand Inst 2002.

[43] BSI. BS EN 13450 Aggregates for railway ballast. Br Stand Inst 2013.

[44] BSI. BS EN 933-1. Tests for geometrical properties of aggregates Part 1: Determination of Particle Size Distribution - Sieving Method. Br Stand Inst 2005;3:1–7.

[45] Kwan C. Geogrid Reinforcement of Railway Ballast. PhD Thesis, University of Nottingham, 2006.

[46] BSI. BS EN 1097-2. Tests for mechanical and physical properties of aggregates. Methods for the determination of resistance to fragmentation. Br Stand Inst 2010.

[47] BSI. BS EN 1097-1. Tests for mechanical and physical properties of aggregates. Determination of the resistance to wear (micro-Deval). Br Stand Inst 2011.

[48] BSI. BS 812-111. Testing aggregates. Methods for determination of ten per cent fines value (TFV). Br Stand Inst 1990.

[49] BSI. BS EN 933-3. Tests for geometrical properties of aggregates. Determination of particle shape. Flakiness index. Br Stand Inst 2012.

[50] BSI. BS EN 933-2. Tests for geometrical properties of aggregates. Determination of particle size distribution. Test sieves, nominal size of apertures. Br Stand Inst 1996.

[51] Indraratna B, Nimbalkar S, Christie D. The Performance of Rail Track Incorporating the Effects Of Ballast Breakage, Confining Pressure and Geosynthetic Reinforcement. Bear Capacit Roads, Railw Airfields 8th Int Conf, 2009.

[52] Indraratna B, Ionescu D, Christie HD. Shear behavior of railway ballast based on large-scale triaxial tests. J Geotech Geoenvironmental Eng 1998;124:439–49.